Journal of Neutron Research 23 (2021) 53–67
DOI 10.3233/JNR-200179
IOS Press

First measurements with the new ^{3}He-filled Monoblock Aluminium Multitube neutron detector developed at the ILL for ANSTO PLATYPUS reflectometer

Luis Abuel [a], Friedl Bartsch [a], Andrew Berry [a], Jean-Claude Buffet [b], Sylvain Cuccaro [b], Patrick van-Esch [b], Bruno Guerard [b], Stephen A. Holt [a], Julien Marchal [b,*], Paolo Mutti [b], Kevin Ollivier [b], Jerome Pentenero [b], Martin Platz [b], Adeline Robert [b], Damien Roulier [b] and James Spedding [a]

[a] *Australian Centre for Neutron Scattering, Australian Nuclear Science and Technology Organisation, New Illawarra Road, Lucas Heights NSW 2234, Australia*
[b] *Institut Laue-Langevin, 71 avenue des Martyrs CS 20156, 38042 GRENOBLE Cedex 9, France*

Abstract. A detector upgrade was carried out on the PLATYPUS instrument dedicated to neutron reflectometry at the Australian Nuclear Science and Technology Organisation (ANSTO). The new detector, developed in the framework of a research collaboration between the ILL and ANSTO, is based on the Monoblock Aluminium Multi-tube (MAM) detector design already in use on several reflectometers and SANS instruments at the ILL. This article provides a technical description of the mechanical design and read-out electronics of the PLATYPUS detector and its commissioning on the PLATYPUS instrument. The main detector performance parameters have been measured and are presented here as well as the characterisation methods and the results of several reflectometry measurements. These measurements show an improvement in experimental data quality resulting from high positional resolution, high detection efficiency and reduced neutron scattering background in the 2.5–19 Å neutron wavelength range used in PLATYPUS instrument.

Keywords: Neutron detector, ^{3}He-based detector, gaseous detector, neutron reflectometry

1. Introduction

Neutron reflectometry enables the study of both hard matter and soft matter phenomena and is integral in tackling cutting-edge scientific problems. Neutron reflectometers require two-dimensional detectors combining both high spatial resolution and high counting rate. The counting rate requirements are very challenging for the future reflectometers instruments of the upcoming European Spallation Source, where ^{10}B detectors are currently being built [12,13], based on the ^{10}B Multi-Blade detector concept [2]. However, the performance of ^{3}He detectors is acceptable for reflectometry experiments in most of the present neutron science facilities. Reflectometry experiments are only marginally impacted by the cost fluctuation and scarcity of ^{3}He since they require a relatively low volume of ^{3}He (typically around 15 litres) to provide high detection efficiency in the thermal neutron energy range over an active area typically around 20 cm by 20 cm.

Neutron detectors based on ZnS scintillators have a fast scintillation decay time component combined to a slower decay time component of the order of several microseconds, whereas the signal development in a ^{3}He detector is

*Corresponding author. E-mail: marchalj@ill.fr.

ten times faster. Li-glass (GS20) scintillators which are also widely used for neutron detection have a very fast decay time of the order of 50 ns but they are also sensitive to gamma rays. On the other hand, ^{3}He proportional chambers provide both high counting rate and high neutron/gamma discrimination capabilities.

At the ILL, for several years, reflectometry instruments such as FIGARO [4] and D17 [14] have benefited from the fast response of two-dimensional position sensitive neutron detectors based on the Monoblock Aluminium Multitube (MAM). Similar detectors, consisting of several Multitube blocks welded together to make larger detectors, have also been installed on instruments dedicated to Small Angle Neutron Scattering (SANS) such as D33 [6] at the ILL or PAXY and PA20 [5] instruments at the Léon Brillouin Laboratory (LLB).

In these detectors, adjacent tubes are machined in a block of aluminium using wire electro-erosion; compared to independent PSDs, these tubes can be fabricated with a smaller section (down to 5 mm pitch) and can be machined side by side with high precision without the need for a complex mechanics to support them. These tubes are usually machined with a rectangular section to enhance the detection efficiency and provide a uniform response across each tube. The position measurement along the tubes being independent from one tube to the others, several tubes can count simultaneous neutrons. This configuration and the simplicity of its design are the main advantages of the Multitube. Other types of ^{3}He-based detectors structures, in particular Multi-Wire-Proportional-Chambers or Microstrip detectors, are still considered for neutron reflectometry to overcome the limit of spatial resolution resulting from the section of the tubes [1].

PLATYPUS is a multipurpose Time-Of-Flight (TOF) neutron reflectometer situated on Cold Guide 3 at the OPAL reactor at ANSTO [7,8,15]. For hard matter studies, PLATYPUS enables investigation of the properties of magnetic materials, including determining the magnetisation of an iron monolayer or of a grain boundary in nickel. PLATYPUS instrument also allows the study of interface roughness and magnetic direction across the interfaces in computer hard-drive read-heads. For soft matter it enables the study of solid-liquid or air-liquid interfaces, including the self-assembly of silicate structures at air-water surfaces, or of the nature and properties of lung surfactants and proteins in membranes.

PLATYPUS was designed with a horizontal sample plane to enable the study of free liquid, solid surfaces and interfaces. This is coupled with a neutron polarisation and analysis system for investigations of magnetic structures. Scattering from free liquid surfaces is achieved via the use of supermirrors to deflect incoming neutron beam down onto the liquid surface, for which two configurations are possible: a double bounce system with fixed deflection angle; and a single bounce mirror mounted on a rotation stage for low angle incident data. For solid interfaces, a sample table on top of a goniometer controls the incident angle and allows positive or negative angles with the outgoing beam being reflected above or below the horizontal respectively. In all cases, standard practice is to track the position of the reflected beam on the detector by means of a height stage such that the beam is always incident in the same region of the detector. The PLATYPUS instrument's scientific research highlights include investigating plasma-polymer coatings for biopassivation, Titania nanoclusters embedded in polymer matrices and a commercial Ni-Ti multilayer system. The detector used during the experiments producing these scientific research highlights was a 2-dimensional MWPC ^{3}He detector which produced high-quality data for many years since its commissioning on the instrument in 2006 [8].

In 2016, a research collaboration between ILL and ANSTO was set-up to upgrade PLATYPUS instrument with a new detector based on MAM concept and fabrication techniques. This project led to the fabrication of a MAM detector with a configuration adapted to the mechanical constraints of PLATYPUS instrument.

2. PLATYPUS MAM detector

The PLATYPUS MAM detector was designed to operate inside the large vacuum tank of the reflectometer instrument at ANSTO. The PLATYPUS detector system consists of three parts:

- a Monoblock Aluminium Multitube detector head filled with ^{3}He
- a vacuum tight mechanical enclosure hosting the air-cooled front-end electronics

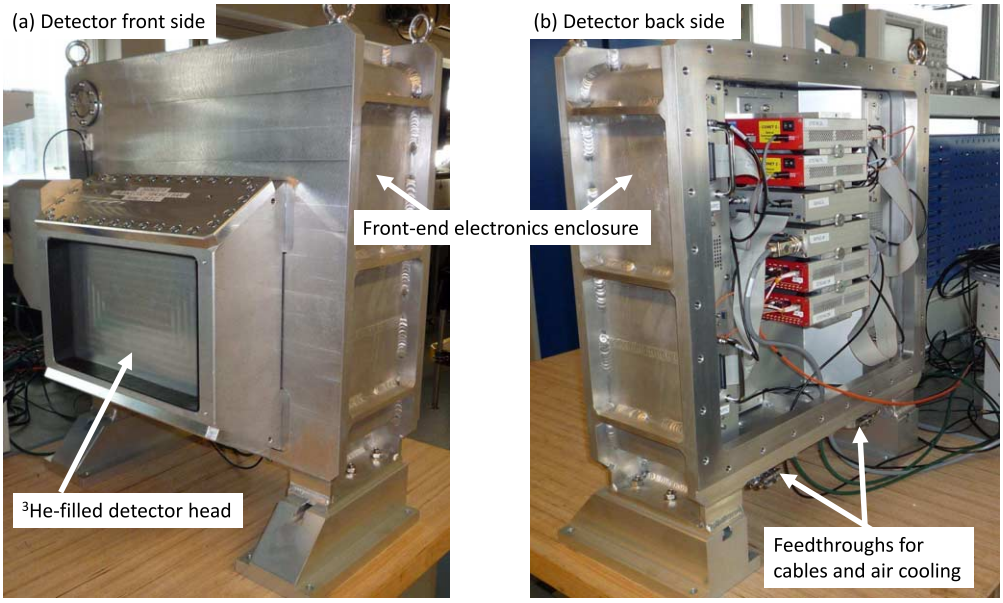

Fig. 1. Photograph of the PLATYPUS MAM detector system showing the ^{3}He-filled detector head (a) and the front-end electronics enclosure (b).

- back-end electronics located outside the vacuum tank and integrated in the data acquisition system of the instrument

The detector head is bolted onto the front of the electronics enclosure as shown in Fig. 1. The total weight of the detector is 120 kg and the overall dimensions are 60 cm (width) × 65 cm (height) × 45 cm (depth). The detector head vessel itself contains 64 adjacent vertical tubes (at a pitch of 5 mm), operated as standard gas proportional counters. These tubes are gathered in 2 adjacent sectors of 32 tubes. Only one 32-tubes sector is operated, the other one serving as a spare. The two sectors share the same gas volume and only one sector is powered at a time even if both sectors are always equipped with their independent read-out electronics. The spare sector is available so that in case of a fault with the main sector, it is possible to translate laterally the detector inside the vacuum tank and power-up the spare sector. The active area of one sector covers 16 cm horizontally by 21 cm vertically.

For each neutron interacting with the detection gas, the front-end electronics compute the coordinates of the interaction point and record the timestamp of the interaction, allowing neutron time-of-flight studies. A fibre optic link is used to transfer detector data from the front-end electronics to the acquisition system located at several tens of meters of the detector which can be moved along a 1 meter range inside the 3.5-meter long vacuum tank of PLATYPUS instrument.

In the axis of the tubes the spatial resolution of 1.5 mm is determined by the pressure of the stopping gas ($ArCO_2$) and the signal processing technique (resistive charge-division along anode wires) whereas the resolution in the direction orthogonal to the tubes is defined by the tube width of 5 mm.

The main characteristics of PLATYPUS detector are summarised in Table 1 and more details regarding the mechanical and electronics read-out design of the detector are given in the next sections.

2.1. Mechanical design

2.1.1. Detector head

The detector head in Fig. 2(a) consists of a vessel body (aluminium block inside which 64 adjacent tubes have been machined) covered by two aluminium plates used to seal the gas volume shared by these 64 tubes. The gas

Table 1
Specifications of PLATYPUS MAM detector

Gas mixture	^{3}He (10 bar) and $ArCO_2$ (5 bar)
Active area	21 cm (height) × 16 cm (width) per detector sector
Spatial resolution	5 mm (hor.) × 1.5 mm (vert.)[1]
Detection efficiency	66% for 2Å neutrons
Number of tubes	32 per detector sector
Tube internal section	4.5 mm (hor.) × 7.5 mm (depth)
Overall dimensions	60 cm (width) × 65 cm (height) × 45 cm (depth)
Detector head volume	1.5 litres (for the 2 detector sectors)

[1]The spatial resolution in the vertical direction is determined by the charge-division electronics. Details on spatial resolution measurements are given in Section 3.2

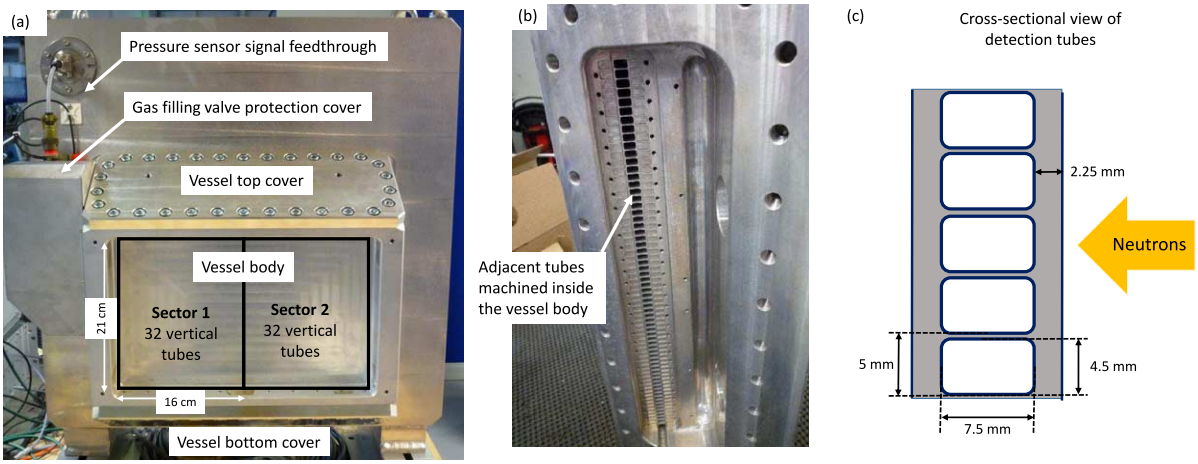

Fig. 2. (a) Photograph of the detector head showing the vessel body (b) adjacent tubes machined inside the vessel body (c) cross-sectional view of the vessel body showing the dimensions of the tubes.

tightness of the detector head is provided by means of metallic gaskets inserted in grooves machined on the surface of the 2 aluminium covers.

The 64 square tubes which were spark-eroded in the aluminium block are shown in Fig. 2(b). These tubes are 21 cm long with a rectangular section of 7.5 mm × 4.5 mm and a separation of 0.5 mm between them, as illustrated in Fig. 2(c). A metallic (anode) resistive wire (not shown in Fig. 2(b)) is stretched inside each tube and the two extremities of each wire are soldered onto a polyimide circuit connecting them electrically to custom multi-pin high-voltage feedthroughs developed for high-pressure applications. During operation a positive voltage of around 2kV is applied to the anode wires in order to amplify (by electron avalanche multiplication) the charge resulting from the neutron interaction process in the detection gas. These electrical signals are transferred via the multi-pin feedthrough directly to the front-end electronics located at the back of the detector head.

The 1.5 litres detector head vessel is designed to operate at a maximum (absolute) pressure of 15 bar. Finite element modelling was performed to confirm that this vessel complies with the European Pressure Equipment Directive 2014/68/EU. The detector head was filled to 15 bar at room temperature with a partial pressure of 10 bar of ^{3}helium, 4.9 bar argon and 0.1 bar of CO_2. A mixture of argon and CO_2 was selected as the stopping gas.

2.1.2. Front-end electronics enclosure

In previous versions of MAM detector systems developed at the ILL, analogue signals produced at the output of pre-amplifiers located in the front-end electronics enclosure were transferred to signal digitisation and processing

modules located in the back-end acquisition system, via individual coaxial cables or RJ45 cables. In the PLATYPUS detector system, cable management was simplified by integrating the signal digitisation and processing units in the front-end electronics enclosure and transferring data via a fibre link to the back-end electronics. However, this approach requires the design of a larger enclosure and also leads to additional power dissipation requirements (50W to be dissipated in the electronics enclosure instead of 2W for 32 tubes).

A large aluminium vessel 60 cm (width) × 65 cm (height) × 30 cm (depth) was manufactured to mount the various front-end electronics boards (described in the next section) performing signal pre-amplification, digitisation and processing. The electronics enclosure is located in the vacuum tank of the instrument and cooling-air is circulated inside the enclosure at a pressure slightly above the atmospheric pressure. During operation, the temperature of the FPGA boards located in the digitizers and monitored by the read-out software stabilises at 50°C and the temperature of the thermocouple mounted onto the digitizer heatsink stabilises at 40°C.

High-vacuum flanges were welded on the electronics enclosure for air-cooling pipes connection, electrical cables and the fibre-optic data link. A large plate can be unbolted at the back of the enclosure to facilitate maintenance work on the front-end electronics. Vacuum tightness is obtained by means of FPM o-ring gaskets and KF-standard feedthroughs. A 75 mm-thick polyethylene block covered on both sides by a 5 mm-thick boron-loaded elastomer sheet (50% SBR/50% boron carbide) is mounted between the detector head and the electronics enclosure to prevent backscattering of neutrons into the detector tubes and to shield the electronics.

2.2. *Read-out electronics*

One of the main features of the PLATYPUS design compared to MAM systems installed previously at ILL or LLB is the integration of the digitising units in the front-end electronics located inside the vacuum tank of the instrument. This has the advantage of reducing the number of air-filled pipes which have to be routed along the movable detector inside the vacuum tank.

2.2.1. *Front-end electronics*

Each 32-tube sector of the detector is equipped with its own front-end electronics including the following components:

- Two decoupling boards (Fig. 3(b)): These boards connect directly to the multi-pin high-voltage feedthrough of the detector head (Fig. 3(a)). They are used to apply High-Voltage to anode wires and to decouple fast signals pulses from the high-voltage DC signal.
- Two pre-amplification boards (Fig. 3(c)): 8-layer 32 channel **P**re**A**mp boards with **UNI**polar outputs (PAUNI) have been designed for this project. They provide 32 charge-sensitive amplifiers with transimpedance gain of 1V/pC and 32 unipolar voltage drivers matching the 2V input range of the digitizers.
- Two digitizers (Fig. 3(d)): The digitization and processing of neutron-induced pulses produced on both sides of each detector tube are performed by CAEN DT5740-D digitizers.[1] The DT5740-D is a 32 Channel 12 bit 62.5 MS/s Desktop Waveform Digitizer with 2 Vpp single ended input dynamics on ERNI SMC connectors. The DT5740-D FPGA firmware was modified by ILL to meet the requirements of the resistive charge division technique used at the ILL [16]. This processing includes digital filtering of the pre-amplified signals produced on both ends of each tube, calculation of the positional information (neutron interaction point along the wire) and transmission of this positional information together with a 48-bit event timestamp. The digital filter takes 12-bit ADU values and outputs 16-bit filtered signal values. A 16-bit detection threshold, adjusted according to the procedure described in Section 3.6, is applied to the sum of the two filtered signals from each tube ("A + B"). The two DT5740-D house USB 2.0 and Optical Link interfaces. The Optical Link, supporting transfer rate of 80 MB/s, is daisy-chained across the two digitizers to transfer data signals to the back-end electronics.

[1] https://www.caen.it/products/dt5740/

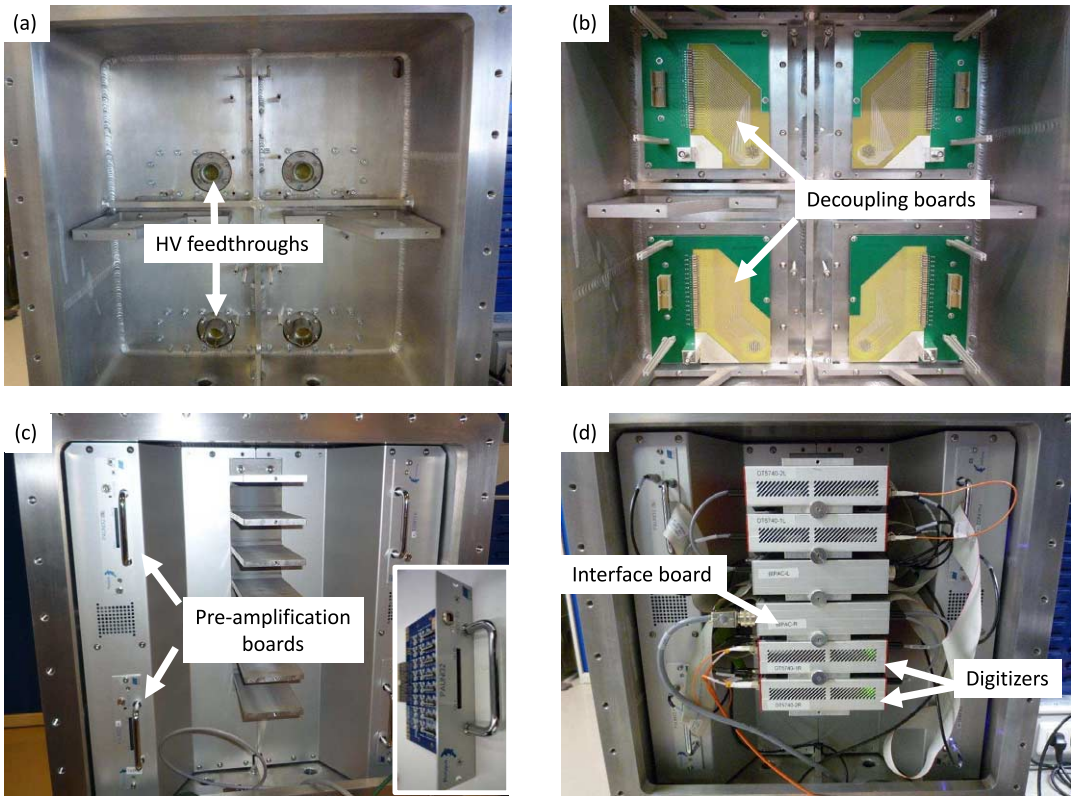

Fig. 3. Front-end electronics at various assembly stages: (a) electronics enclosure with HV feedthroughs, (b) decoupling boards connnected to the HV feedthroughs, (c) pre-amplification cards connected to the decoupling boards, (d) digitizers and interface boards mounted in the enclosure.

- An interface board (Fig. 3(d)): The BIPAC (**B**ox **I**nterface for **PA**uni board and **C**aen DT5740 board) distributes power, clock and gate signals to the various boards and reroute the outputs of the pre-amplification boards so that signals produced at both ends of a tube are connected to the same digitizer, since each 32-channel digitizer can process the 16 pairs of signals (top and bottom) produced by 16 tubes.

2.2.2. *Back-end electronics*

Data read-out is performed by a CAEN PCI-E connect controller A3818B[2] with CONNECT 2 CAEN proprietary protocol. The controller A3818B is a 32-bit 33 MHz PCI-E card, which allows the control, through a standard PC, of up to 8 CAEN Optical Slave Cards per optical link. The 2 DT5740-D digitizers are continuously processing and transmitting neutron position and timestamp data from the 32 tubes. Neutron events data are coded over 3 words of 32 bits including 48 bits for the timestamp, 16 bits for the pulse height at one side of the tube ("A"), 16 bits for the sum of the pulse heights at both sides of the tube ("A + B"), 4 bits for the tube number and some extra bits for the status of various acquisition system flags. The back-end electronics decodes the data and uses the "A" an "A + B" information to calculate the neutron interaction position (A/A + B) along the tube, and re-bins it into 1024 pixels.

The data are transferred via a 80 MB/s fibre optic link and the DAQ system can handle sustained transfer rates up to 500 Mbit/s corresponding to a count-rate of ∼5 MHz with 96-bits events and data packets overheads (tested with a pulse generator). During the tests with neutrons, global count rates up to 500 kHz were reached without any limitation or dead-time introduced by the DAQ system.

[2] https://www.caen.it/products/a3818/

In order to synchronise the acquisition with other equipment such as beam choppers or monitors, a TTL Gate signal is sent to the digitizers and a flag is set to 1 in the data when the Gate signal level is high.

2.2.3. Acquisition control

Experiment and acquisition control is performed by the Histogram Memory Server (HMS) which was custom-built at ANSTO within the GumTree integrated scientific experiment environment [9]. A custom device driver was written to integrate the A3818B PCI-E card with the HMS, enabling the HMS to configure the two DT5740-D digitizers and accept or ignore the continuously streamed neutron data. The time, position, energy and gate data from neutron pulses are then stored in arrays and made available for data reduction.

3. PLATYPUS detector characterisation with neutrons

The performance of PLATYPUS detector was evaluated with neutrons on CT2 test instrument which has been used at ILL to characterize various types of detector technologies [3,11]. The beam of neutrons with 2.5 Å wavelength was produced with a Highly Oriented Pyrolytic Graphite monochromator. Sintered B4C slits were used to define the size of the neutron beam and the neutron flux was varied by inserting various PMMA sheet in front of the slits. The next sections describe the experimental method and the results obtained when measuring various detector performance parameters.

3.1. Image uniformity and background counts

A PMMA sheet was used to scatter the main neutron beam to produce a uniform illumination on the detector and acquire a flat-field image. This flat-field image shown in Fig. 4(a) was projected along each dimension of the detector in Fig. 4(b) and (c). The uniformity of the detector response obtained across tubes is better than +/−0.3%. It can also be noted in Fig. 4(b) that the illumination used for this flat-field measurement was not perfectly uniform (slope visible between bins 200–900). This is because the flat-field illumination was performed with a water sample producing 4π scattering and the detector was raised vertically out of the direct beam, meaning that the effect of the solid-angle on the uniformity of the flat-field illumination was more important in the vertical direction. Images were also acquired without neutron beam to confirm the absence of spurious signal pulses and confirm that the signal discrimination threshold settings of the detection channels were high enough to suppress the electronics noise of pre-amplification channels. These background images acquired during a reactor shutdown period at ILL resulted in a background count-rate below 1 Hz per sector of 32 tubes.

3.2. Spatial resolution

The spatial resolution of the detector was measured by acquiring images of 0.5 mm slits machined in a cadmium mask mounted between two aluminium plates. The mask mounted on the detector front window is shown in Fig. 5 (the 0.7 mm cadmium sheet was inserted between 2 plates of aluminium so that high precision could be achieved when machining the slits). Gaussian fitting was applied to the images obtained at a high-voltage of 2250V and resulted in a measured spatial resolution of 1.5 mm FWHM after deconvolving the 0.5 mm width of the slits. This value corresponds to the theoretical spatial resolution expected for the pressure (5 bar) of the stopping gas ($ArCO_2$) in the detector [10]. The small offset (<5%) visible at the bottom of the slit profiles (compared to the Gaussian fits) is probably due to internal scattering in the detector. Measurements were also repeated at a lower high-voltage of 2150V and resulted in a spatial resolution of 1.8 mm FWHM. This is expected since the position resolution obtained by charge-division is directly related to the SNR, which is itself dependent on the gas amplification gain and therefore the high-voltage applied to anode wires. For HV = 2250V, the contribution of electronic noise to the spatial resolution becomes marginal compared to the range of protons and tritons in the gas mixture.

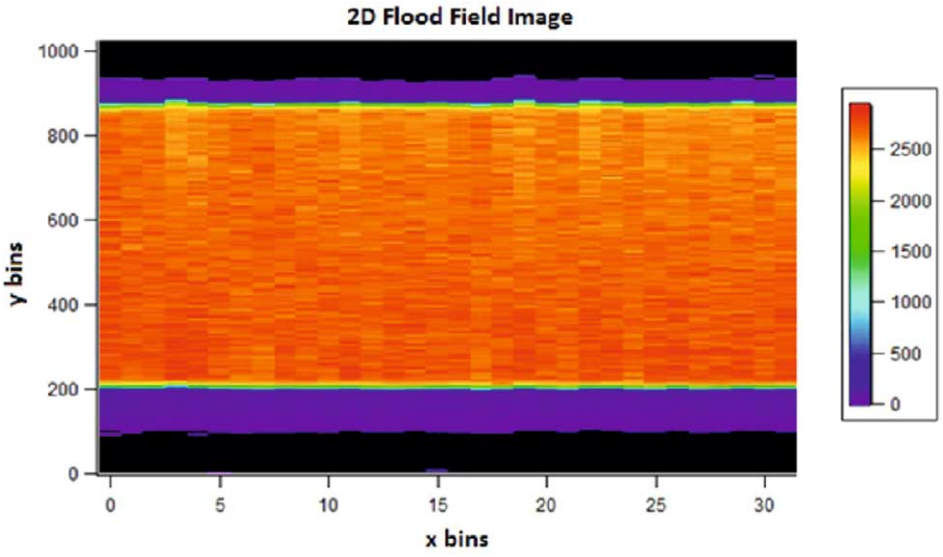

(a)

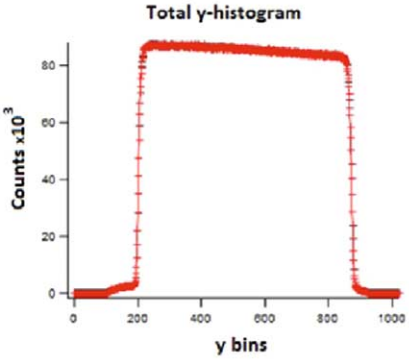

(b)

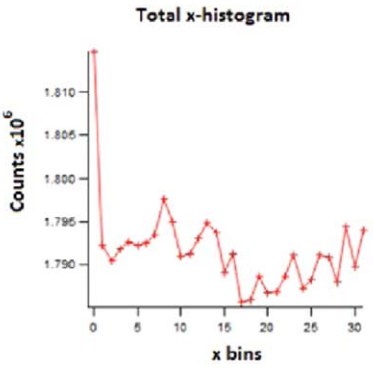

(c)

Fig. 4. (a) A two-dimensional flood-field image acquired on the PLATYPUS instrument showing uniform illumination and response from the detector; (b) a histogram of all tubes showing uniform y-directional response from the detector; (c) a histogram across all bins showing a uniform response from each tube in the detector. A slightly elevated response in tube 0 is caused by reflection from the metallic detector lip.

3.3. Gain uniformity

The height of neutron-induced pulses produced on both sides of the tubes is recorded by the digitizers in order to calculate the position of the neutron interaction point. The output data of the digitizers contains not only the calculated position but also the pulse heights, allowing for pulse-height spectra to be plotted for each tube by the acquisition system. These spectra can be used to check the uniformity of the amplification gain between tubes. Pulse-height spectra obtained under flood-field illumination of the detector with 2.5 Å neutrons resulted in a maximum gain deviation of 2% across the 32 tubes of the detector. It should be noted that in all the measurements presented in this paper as well as when the detector is in operation on PLATYPUS instrument, the same detection threshold is applied to the 32 channels even if it is possible to upload individual thresholds for each channel to correct any strong gain variation between channels. However this is not necessary to use this feature of the acquisition set-up because of the good uniformity between amplification gains observed on the PLATYPUS detector. This

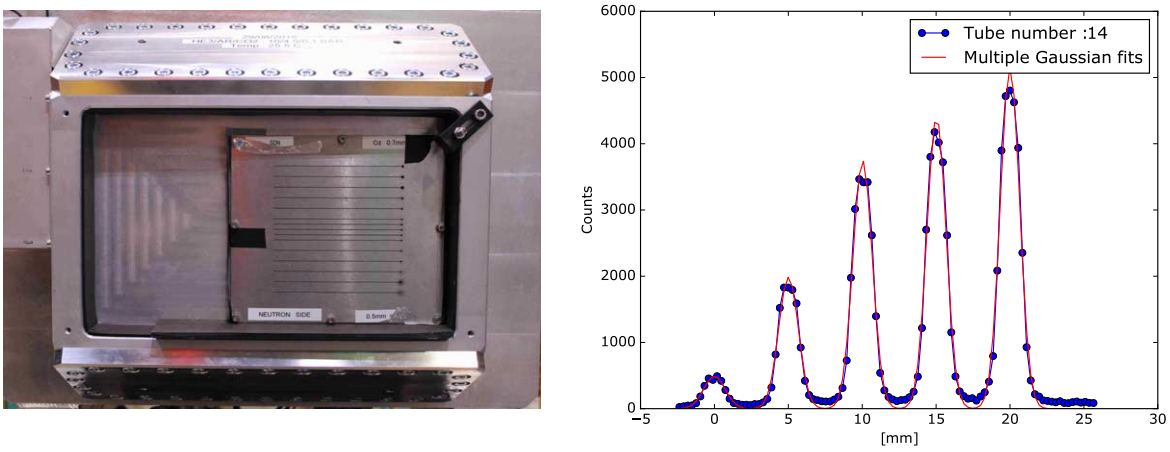

(a) (b)

Fig. 5. (a) Cadmium slit-mask used to measure the spatial resolution of the detector in the vertical direction; (b) example of Gaussian fits performed on the position data obtained on one tube behind the cadmium mask.

gain uniformity results from the high mechanical precision achieved by the wire electro-erosion technique used to machine the tubes in the vessel body and the precision achieved in stretching and crimping anode wires along the central axis of each tube.

3.4. Count rate linearity

In gas-filled proportional chambers, the linearity of the counting response can be affected by signal pile-up effects or by space-charge effects occurring when a high neutron flux is localised on a small region of the detector. The second effect should be dominant when the counting rate on one tube does not exceed 50 kHz, which is the case for most reflectometry experiments. To investigate the space-charge effect, the detector was exposed to a 1 cm-high neutron beam covering 10 tubes. This narrow beam was obtained using a pair of cadmium slits collimating the direct beam and 2-dimensional images were acquired for various thicknesses of PMMA attenuators.

The measured count-rate was plotted as a function of attenuator thickness in Fig. 6 and a linear count-rate was observed up to 20 kHz per tube obtained without any attenuators. This local count-rate of 40 kHz/cm^2 achieved without significant count loss (<1%) was limited only by the neutron flux available on CT2 instrument in the specific experimental configuration used to test the detector. This result was obtained at a High-Voltage of 2150V, corresponding to a 1.8 mm spatial resolution (cf Section 3.2). At higher High-Voltage values, such as HV = 2250V corresponding to a spatial resolution of 1.5 mm FWHM, count-loss would be higher but priority was given to low HV operation during the tests since low-gain operation is more favourable to the long-term stability of the detector.

Count-rate linearity in a multi-channel gas-filled detector can also be limited by global effects resulting from pulse pile-up, electronics processing of many channels at a time and the bandwidth of data transmission media. To investigate the global count rate linearity of the detector, a large neutron beam of 5 cm (vert.) × 5 cm (hor.) covering 10 tubes was attenuated with various thicknesses of PMMA sheet and the count-rate measured by the detector was plotted as a function of attenuator thickness. The global count-rate measured using this method was linear up to 500 kHz over a large surface (5 cm × 5 cm) of the detector.

3.5. Position linearity

The positions of neutron interactions in the detector are computed from signals produced at both ends of each tube, using the resistive charge division approach. The precision of this position calculation is affected by gain and

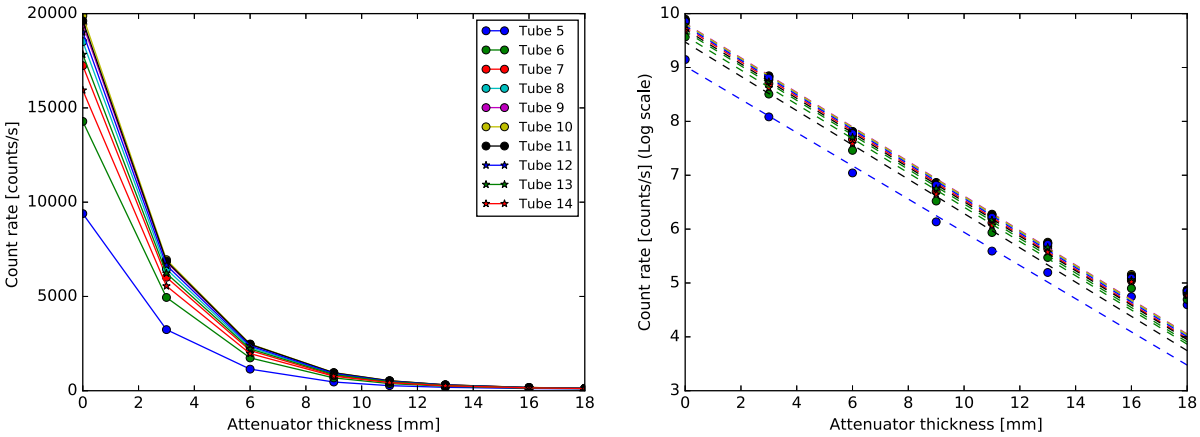

Fig. 6. Count-rate linearity measurement: (a) individual tube count-rate as a function of attenuator thickness. (b) Linear fit to the data in log scale, excluding the points corresponding to high attenuator thickness (with low counting statistics).

offset variations between electronics channels and additional resistances present at both ends of the tubes, due the electrical connections. These effects lead to a distortion of the 2-dimensional image as shown in the uncalibrated image in Fig. 7.

Image distortion is corrected by computing gain and offset correction coefficients for each tube. These coefficients are applied to neutron position data in the digitizer firmware. The accuracy of the geometrical correction was investigated by using a cadmium calibration mask consisting of a central slit (5 mm wide) between 2 edges located at 53 mm from the central slit. On the image of Fig. 7(a), the pixel position corresponding to the top edge and the pixel position corresponding to the bottom edge of the mask are calculated for each tube. Knowing the physical distance between these two positions (106 mm in our case), it is possible to compute the 2 coefficients required for linear correction of the position data. Figure 7(b) shows the mask image after correction. One way of confirming that this linear correction is effective consists in plotting the position of the central slit (which was not used for the calculation of the correction coefficients) before and after correction. The maximum position error (maximum distance between the measured slit position and the physical slit position half way between top and bottom edges) is reduced from 3.5 mm (no correction) to 0.4 mm (after correction).

3.6. Gamma-ray rejection

Gamma-ray rejection could not be measured precisely on CT2 test instrument. However spectra recorded during the threshold adjustment procedure, described below, show that at the recommended HV, the detection threshold can be set in the valley of the Pulse Height Spectrum between gamma-ray pulse heights and neutron pulse heights, indicating that the detector benefits fully from the advantage of ^{3}He-based detectors in terms of gamma-ray rejection.

Threshold adjustment was performed by plotting Pulse Height Spectra for various thresholds values as shown in Fig. 8. The threshold value was increased by steps of 500 ADUs via the acquisition software at the operating voltage of 2150V. The plots show the valley between gamma rays and neutron pulse heights which is characteristic of ^{3}He-filled detectors. The detection threshold was set at the centre of this valley. This corresponds to a threshold of 3700 ADUs at a HV of 2150V and optimum digital filter settings. The same method was used to determine the optimum threshold of 2700 ADUs at the higher HV of 2250V corresponding to an improved spatial resolution of 1.5 mm FWHM.

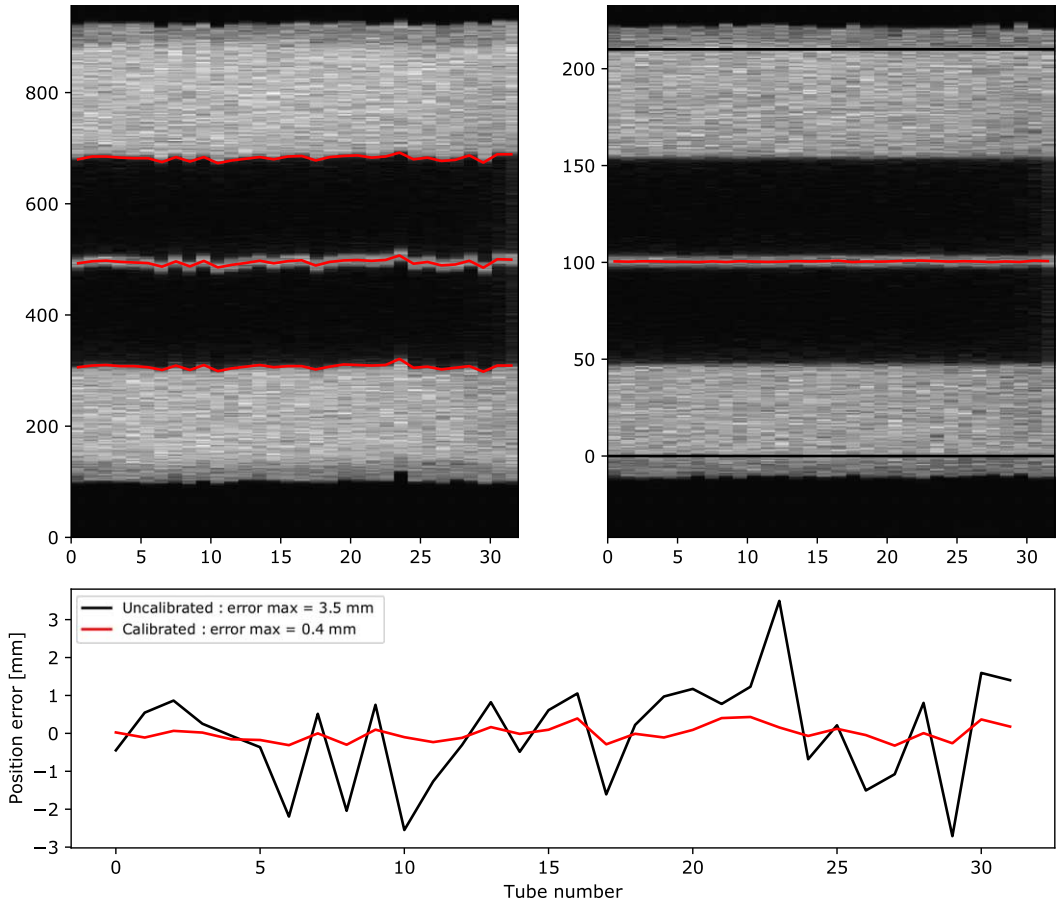

Fig. 7. Position linearity correction: (a) uncalibrated mask image; (b) mask image after applying linear correction coefficients obtained with top and bottom edge positions; (c) position error reduction observed on central slit image after linear correction.

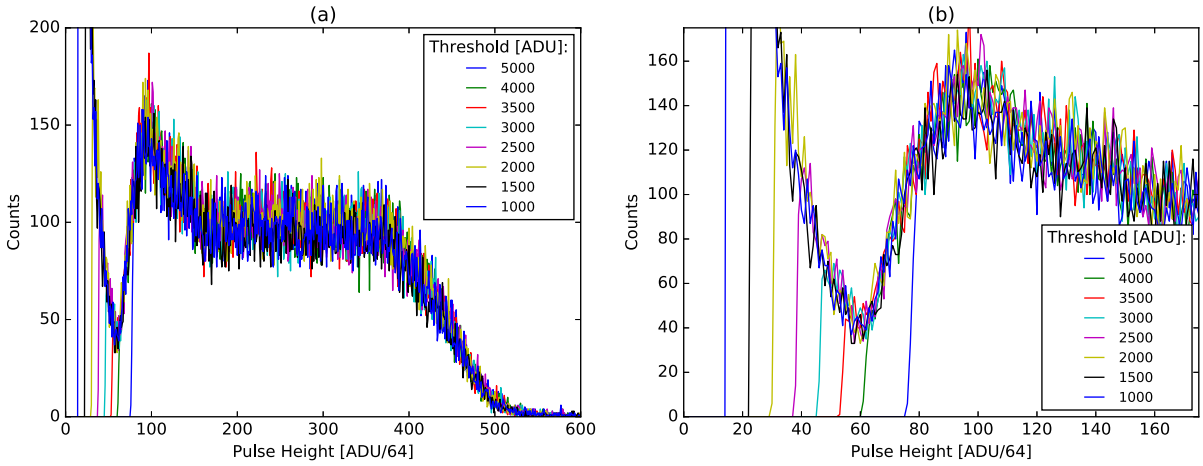

Fig. 8. Threshold adjustement: (a) pulse height spectra recorded at various threshold settings for HV = 2150 V; (b) close-up view showing the valley between gamma-ray and neutron pulse heights in the spectra.

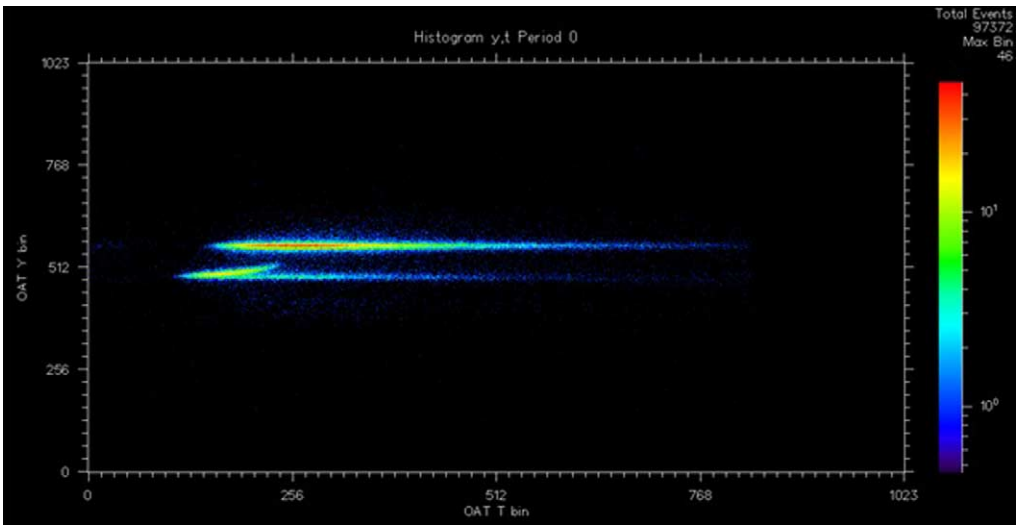

Fig. 9. A time of flight histogram showing reflection data from a plain silicon wafer.

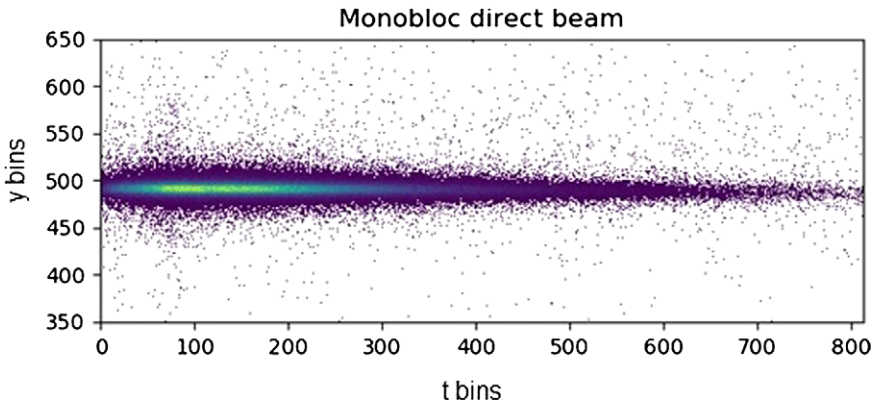

Fig. 10. Vertical position versus time response for the neutron pulse, as measured by the new Monoblock Aluminium Multitube detector. The y-axis represents approximately half the detector y-range.

4. Experimental data from PLATYPUS instrument

First reflection experiments were performed to demonstrate the data quality of the new PLATYPUS detector, using neutrons from the OPAL reactor's CG3 cold neutron beam, while rotating choppers and collimating slits were used to create a pulsed, collimated neutron spectrum. Figure 9 shows a time of flight histogram of neutron reflection data from a plain silicon wafer, acquired with the MAM detector. On this image, the upper line represents the reflected beam, while the lower line represent the direct beam transmitted through the silicon sample. Finally, the slightly curved line between the two shows the refracted beam.

The high spatial resolution (1.8 mm in the vertical direction) of the MAM detector combined to its high timing resolution result in a very precise y-registration of events. This positional and timing resolution is illustrated in Fig. 10, plotting the vertical position of neutron events versus their timestamp while the MAM detector was illuminated with the direct beam on PLATYPUS instrument.

Comparative datasets were collected on a multilayer Bragg mirror film consisting of 25 bilayers of Ni and Ti deposited on float glass under the same conditions with the MWPC detector and then the MAM detector. These

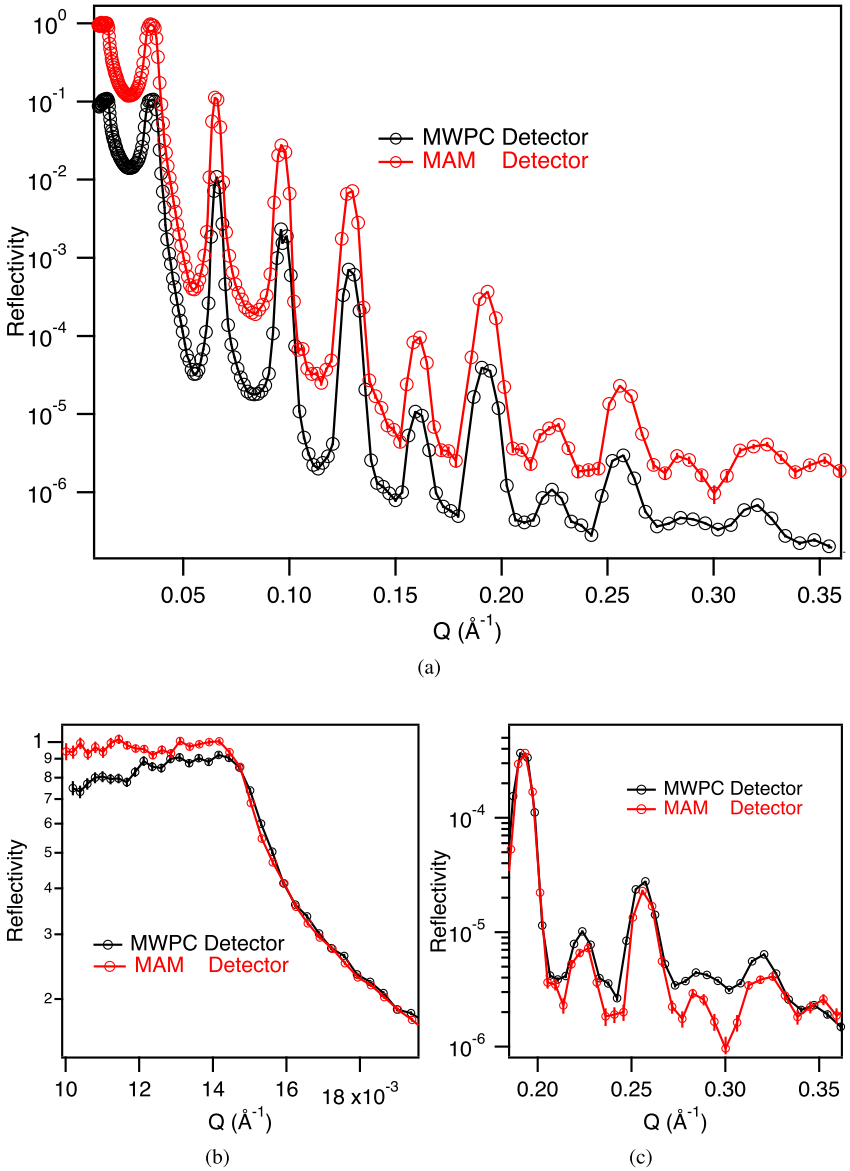

Fig. 11. (a) Data collected on the PLATYPUS instrument using the previous MWPC detector and the new MAM detector (the two dataset were offset for clarity). Reflection data are from a multilayer Bragg mirror film consisting of 25 bilayers of Ni and Ti deposited on float glass. (b) Close-up view on the lower Q region corresponding to longer wavelengths (no offset). (c) Close-up view on the higher Q region corresponding to shorter wavelengths (no offset).

runs consisted of the final and first datasets collected on each detector respectively. Data was collected at three incident angle settings, 0.8, 3.4 and 5.0 degrees. Direct beams through air were recorded for each angle with instrument settings corresponding to that for the data collection. Data was reduced using the Slim package which essentially divided the reflected data through by the direct beam spectrum and rebinned to the defined instrument resolution. Individual angles were then stitched together into a final single dataset.

Figure 11(a) shows the full Q range with the datasets offset for clarity. The agreement between datasets appears to be very good. Closer inspection though reveals some variations at low and high Q values. In Fig. 11(b) it can be

Table 2
Detector/monitor count rates ratio as a function of detector type

Detector	Angle	Collection	Time (s)	Detector Counts	Monitor Counts	Detector (counts/s)	Monitor (counts/s)	Detector/Monitor
MWPC	0.8	Reflection	600	3.75E+06	4.74E+06	6.25E+03	7.91E+03	7.90E–01
MWPC	3.4	Reflection	3600	4.81E+06	5.51E+07	1.34E+03	1.53E+04	8.73E–02
MWPC	5	Reflection	9921.8	2.48E+06	1.52E+08	2.50E+02	1.53E+04	1.63E–02
MAM	0.8	Reflection	600	8.58E+06	4.47E+06	1.43E+04	7.46E+03	1.92E+00
MAM	3.4	Reflection	1800	5.24E+06	2.56E+07	2.91E+03	1.42E+04	2.04E–01
MAM	5	Reflection	3600	2.46E+06	5.11E+07	6.83E+02	1.42E+04	4.81E–02

seen that there is excellent agreement above the critical edge but that there is a divergence in the datasets below this position where the data from the MAM detector is flat but the data from the MWPC detector slopes down slightly. The beam footprint was much smaller than the sample size so the slightly lower reflectivity at the critical edge is not an artefact from data collection. It may be due to the absorption or scatter of long wavelength neutrons by the thicker window on the MWPC detector. At high Q values, in Fig. 11(c), it can be seen that the MAM dataset has an inherently lower background and better defined peaks at the higher Q values. This region of the data is determined by the shorter wavelength neutrons where the MAM detector has a significantly higher detection efficiency.

When one examines the number of counts and counting time for the data presented in Fig. 9 greater differences in performance become apparent. Table 2 presents the total counts and counting time for both detectors when reflection data were collected. In all cases the same slits sizes were used for the same angles. It can be noted that there is some small variation in monitor counts where the data collection times are equivalent, this is due to variations in reactor power as the data were collected in different cycles. The same monitor is used for all data collections. Despite the MAM detector counting for less than half the time, the statistics at high Q (5° angle) are comparable with lower inherent background. It can be seen from the table that the detector count rate (in counts per second) from low to high angle is 6.25E+03, 1.34E+03 and 2.50E+02 for the MWPC whereas for the MAM detector the same configuration results in count rates of 1.43E+04, 2.91E+03 and 6.83E+02 more than double that observed for the MWPC detector. The final column of the table lists the ratio of detector to monitor counts which will correct for variations in reactor power between the different cycles. For the MWPC we see ratios of 7.90E–01, 8.73E–02 and 1.63E–02 versus 1.92E+00, 2.04E–01 and 4.81E–02 for the MAM suggesting a performance ratio of ca 2.4.

5. Conclusion

A new Monoblock Aluminium Multitube detector has been developped for the PLATYPUS reflectometer at ANSTO. The mechanical design of the front-end detector is based on the concept of rectangular position-sensitive proportional tubes precisely machined side by side in a single block of aluminium. This concept has already been used in several reflectometry detectors at ILL as well as several SANS detectors in various reactor-based neutron research organisations. The geometry of the detector was adapted to the requirements of the PLATYPUS instrument. At the detector High-Voltage used on PLATYPUS instrument, the detector provides a spatial resolution of 1.8 mm in the vertical direction along the detection tubes and 5 mm in the direction perpendicular to the tubes. A higher spatial resolution down to 1.5 mm in the vertical direction was also achieved at a higher High-Voltage. The overall mechanical design was optimised to fit the existing detector support inside PLATYPUS vacuum tank. The read-out electronics of this detector includes a signal processing stage based on commercial digitizers with custom firmware. These digitizers are mounted in an air-cooled electronics enclosure located at the back of the detector front-end, inside the PLATYPUS vacuum tank. The first reflectometry experiments performed at ANSTO with the new MAM detector demonstrated a high signal to background ratio of reflected data resulting from the high detection efficiency and the thin aluminium entrance window of the MAM detector.

Acknowledgements

The authors are grateful to Isabelle Petit and Lilian Pereira Bahia from the ILL who supervised administrative aspects of this research collaboration between the two neutron science institutes. We thank Valerie Brachet for supervising the packaging and shipment of the detector system from ILL to ANSTO. The expertise of Jérôme Locatelli from ILL was very much appreciated when setting-up the linux-based environment of the detector data acquisition system at the start of the project. ANSTO is grateful to Kenneth Kwok for developing the CAEN device driver that enabled the new hardware to be integrated into ANSTO's existing data acquisition software, and is also especially grateful to Andrew Nelson, Anton LeBrun and the ACNS Electrical and Mechanical technicians for their careful and professional installation of the new MAM detector.

References

[1] https://sine2020.eu/about/the-road-to-ess/msgcs.html.
[2] J.C. Buffet et al., Study of a 10B-based Multi-Blade detector for neutron scattering science, *IEEE Nucl. Sci. Symp. Med. Im. Conf. Rec.* **171** (2012).
[3] J.C. Buffet et al., Characterisation of a neutron diffraction detector prototype based on the Trench-MWPC technology, *JINST* **12** (2017), C12009.
[4] R.A. Campbell, H.P. Wacklin, I. Sutton, R. Cubitt and G. Fragneto, *Eur. Phys. J. Plus* **126** (2011), 107. doi:10.1140/epjp/i2011-11107-8.
[5] G. Chaboussant et al., PA20: A new SANS and GISANS for soft matter, material and magnetism, *J. of Physics: Conference Series* **340** (2012), 012002.
[6] C. Dewhurst et al., The small-angle neutron scattering instrument D33 at the Institut Laue Langevin, *J. Appl. Cryst.* **49** (2016), 1–14. doi:10.1107/S1600576715021792.
[7] M. James, A. Nelson, A. Brule and J.C. Schulz, PLATYPUS: A time-of-flight neutron reflectometer at Australia's new research reactor, *J. Neutron Res.* **14** (2006), 91–108. doi:10.1080/10238160500472688.
[8] M. James, A. Nelson, S.A. Holt, T. Saerbeck, W.A. Hamilton and F. Klose, The multipurpose time-of-flight neutron reflectometer PLATYPUS at Australia's OPAL reactor, *Nuclear Inst. and Methods in Physics Research A* **632** (2011), 112–123. doi:10.1016/j.nima.2010.12.075.
[9] T. Lam et al., GumTree – an integrated scientific experiment environment, *Phys. B: Condensed Matter* **385–386** (2006), 1330–1332. doi:10.1016/j.physb.2006.06.069.
[10] A. Oed, Detectors for thermal neutrons, *Nucl. Instr. Meth. Phys. Res. A* **525** (2004), 62–68. doi:10.1016/j.nima.2004.03.025.
[11] F. Piscitelli, Novel boron 10-based detectors for neutron scattering science, *Eur. Phys. J. Plus* **130** (2015), 27.
[12] F. Piscitelli et al., Study of high spatial resolution ^{10}B-based thermal neutron detector for application in neutron reflectometry: The Multi-Blade prototype, *JINST* **9** (2014), P03007.
[13] F. Piscitelli et al., Characterisation of the Multi-Blade 10B-based detector at the CRISP reflectometer at ISIS for neutron reflectometry at ESS, *JINST* **13** (2018), P05009.
[14] T. Saerbeck et al., Recent upgrades of the neutron reflectometer D17 at ILL, *J. Appl. Cryst.* **51** (2018), 249–256. doi:10.1107/S160057671800239X.
[15] T. Saerbeck, F. Klose, A.P. Le Brun, J. Füzi, A. Brule, A. Nelson, S.A. Holt and M. James, Polarization "down under": The polarized time-of-flight neutron reflectometer PLATYPUS, *Rev. Sci. Instrum.* **83** (2012), 081301. doi:10.1063/1.4738579.
[16] P. Van Esch et al., Design criteria for electronics for resistive charge division in thermal neutron detection, *Nucl. Instr. Meth. Phys. Res. A* **526** (2004), 493–500. doi:10.1016/j.nima.2004.02.024.